








# On the Parameters of the Spherically Symmetric Parameterized Rezzolla–Zhidenko Spacetime through Solar System Tests, the Orbit of the S2 Star about Sgr A\*, and Quasiperiodic Oscillations

Sanjar Shaymatov<sup>1,2,3,4</sup>, Bobomurat Ahmedov<sup>3,4,5</sup> , Mariafelicia De Laurentis<sup>6,7</sup> , Mubasher Jamil<sup>8</sup> , Qiang Wu<sup>1,9</sup> , Anzhong Wang<sup>10</sup> , and Mustapha Azreg-Aïnou<sup>11</sup>

<sup>1</sup> Institute for Theoretical Physics and Cosmology, Zhejiang University of Technology, Hangzhou 310023, People's Republic of China; [wuq@zjut.edu.cn](mailto:wuq@zjut.edu.cn)

<sup>2</sup> Central Asian University, Milliy Bog St. 264, Tashkent 111221, Uzbekistan

<sup>3</sup> Institute of Fundamental and Applied Research, National Research University TIAME, Kori Niyoziy 39, Tashkent 100000, Uzbekistan

<sup>4</sup> National University of Uzbekistan, Tashkent 100174, Uzbekistan

<sup>5</sup> Ulugh Beg Astronomical Institute, Astronomy St. 33, Tashkent 100052, Uzbekistan

<sup>6</sup> Dipartimento di Fisica, Università di Napoli “Federico II”, Complesso Universitario di Monte Sant’Angelo, Edificio G, Via Cinthia, I-80126 Napoli, Italy

<sup>7</sup> INFN Sezione di Napoli, Complesso Universitario di Monte Sant’Angelo, Edificio G, Via Cinthia, I-80126 Napoli, Italy

<sup>8</sup> School of Natural Sciences, National University of Sciences and Technology, Islamabad 44000, Pakistan

<sup>9</sup> United Center for Gravitational Wave Physics (UCGWP), Zhejiang University of Technology, Hangzhou, 310023, People's Republic of China

<sup>10</sup> GCAP-CASPER, Physics Department, Baylor University, Waco, TX 76798-7316, USA

<sup>11</sup> Engineering Faculty, Başkent University, Bağlıca Campus, 06790-Ankara, Turkey

Received 2023 July 25; revised 2023 September 16; accepted 2023 September 22; published 2023 November 28

## Abstract

In this paper, we find the higher-order expansion parameters  $\alpha$  and  $\lambda$  of spherically symmetric parameterized Rezzolla–Zhidenko (PRZ) spacetime by using its functions of the radial coordinate. We subject the parameters of this spacetime to classical tests, including weak gravitational field effects in the solar system, observations of the S2 star that is located in the star cluster close to the Sgr A\*, and of the frequencies of selected microquasars. Based on this spherically symmetric spacetime, we perform the analytic calculations for solar system effects such as perihelion shift, light deflection, and gravitational time delay to determine limits on the parameters by using observational data. We restrict our attention to the limits on the two higher-order expansion parameters  $\alpha$  and  $\lambda$  that survive at the horizon or near the horizon of spherically symmetric metrics. The properties of the expansion of these two small parameters in PRZ parameterization are discussed. We further apply Markov Chain Monte Carlo simulations to analyze and obtain the limits on the expansion parameters by using observations of the phenomena of the S2 star. Finally, we consider the epicyclic motions and derive analytic expressions of the epicyclic frequencies. Applying these expressions to the quasiperiodic oscillations of selected microquasars allows us to set further limits on the parameters of the PRZ spacetime. Our results demonstrate that the higher-order expansion parameters can be given in the range  $\alpha, \lambda = (-0.09, 0.09)$  and of order  $\sim 10^{-2}$  as a consequence of three different tests and observations.

*Unified Astronomy Thesaurus concepts:* [Black holes \(162\)](#); [X-ray binary stars \(1811\)](#)

## 1. Introduction

General relativity (GR), formulated by Albert Einstein in 1915, introduced a new concept of space and time by showing that massive objects cause a distortion in spacetime that is felt as gravity (Einstein 1916). In this way, Einstein’s theory predicts, for example, that light travels in curved paths near massive objects, and one consequence is the observation of the Einstein Cross. The Einstein Cross are four different images of a distant galaxy that lies behind a nearer massive object, and whose light is distorted by it. Other well-known effects of GR are the observed gradual change in Mercury’s orbit due to spacetime curvature around the massive Sun, or the gravitational redshift, which is the displacement to the red of lines in the spectrum of the Sun due to its gravitational field.

So far, all gravitational field effects in the solar system (SS) in the weak-field approximation and in binary systems are well described by means of GR (Will 1993; Will 2001). V. Kagramanova et al. (Kagramanova et al. 2006) studied SS

effects in Schwarzschild–de Sitter spacetime. Based on this spacetime, they calculated SS effects such as gravitational redshift, light deflection, gravitational time delay, perihelion shift, geodesic or de Sitter precession, and the influence of the cosmological parameter  $\Lambda$  on Doppler measurements that were used to determine the velocity of the Pioneer 10 and 11 spacecraft. Grumiller later constructed an effective model for the gravity of a central object at large scales (Grumiller 2010). To leading order in the large-radius expansion, he found a cosmological constant, called Rindler acceleration, which sets the physical scales and subleading terms. In the past decades, hundreds of experiments and observations have been performed to confirm Einstein’s theory. Some of these experiments and observations are entirely new tests, probing aspects of gravity that Einstein himself had never conceived of. One of the first exciting validations of GR was the observation of the binary system PSR B1913+16, where it was observed that the orbits of the two stars were shrinking (Hulse & Taylor 1974, 1975). This shrinkage is caused by the loss of orbital energy due to gravitational radiation, which is a traveling ripple in spacetime that is predicted by Einstein’s GR theory, but was never previously verified. Very recently, we have witnessed numerous gravitational wave observations



Original content from this work may be used under the terms of the [Creative Commons Attribution 4.0 licence](#). Any further distribution of this work must maintain attribution to the author(s) and the title of the work, journal citation and DOI.

by the LIGO-Virgo instruments (Abbott et al. 2016), the study of stars orbiting the supermassive black hole at the center of the Milky Way (Ghez et al. 1998), and the stunning image of the black hole shadow in the galaxy M87 (Akiyama et al. 2019a, 2019b). In this vast and diverse array of measurements, we did not find a single deviation from the predictions of GR. The string of successes of GR experimentally and observationally is rather astounding. After more than 100 yr, it seems that Einstein is still right.

Will this perfect record hold up? We do know, for example, that the expansion of the Universe is speeding up, not slowing down, as recent observations predict (Di Valentino et al. 2021). Will this require a radical new theory of gravity, or can we make do with a very slight tweak of GR? As we make better observations of black holes, neutron stars, and gravitational waves, will the theory still pass the test?

Both dark matter and dark energy in the observable Universe have given rise to new alternative theories of gravity because the classical Einstein GR is not sufficient to explain these observations (Rubin et al. 1980; Wetterich 1988; Persic et al. 1996; Kiselev 2003; Peebles & Ratra 2003; Spergel et al. 2007; Caldwell & Kamionkowski 2009; Akiyama et al. 2019a, 2019b). These modified theories of gravity have provided very potent tests of probing new exact solutions for gravitational objects (Hellerman et al. 2001; Kiselev 2003; Peebles & Ratra 2003). Thus, it turns out that it is very crucial to parameterize the solutions of gravitational field equations. In this framework, a new parametric framework able to mimic spacetime geometry of generic static spherically symmetric black holes was proposed in Rezzolla & Zhidenko (2014). The peculiarity of this approach is that an expansion of continuous fractions is used by compacting the radial coordinate, which allows a fast convergence. Recently, the Rezzolla–Zhidenko (PRZ) spacetime has been studied as a model of a black hole undergoing spherical accretion of matter and dust (Yang et al. 2021) and as a model of the Galactic center S-stars and distinct pulsars through test-particle dynamics (De Laurentis et al. 2018). The PRZ spacetime can also be regarded as a model of the quasiperiodic oscillations observed in microquasars, with the low-mass X-ray binary systems consisting of either a black hole or a neutron star and of X-ray data from compact objects (Bambi 2012; Bambi et al. 2016; Tripathi et al. 2019). These models would play an important role in testing remarkable aspects of PRZ spacetime and in constraining the magnitude of its expansion parameters. Generally, the observed quasiperiodic oscillations (QPOs) in Galactic microquasars are determined by the ratio 3:2 (Kluźniak & Abramowicz 2001), which are either referred to as high-frequency (HF) or low-frequency (LF) QPOs with the X-ray power. The HF QPOs are usually referred to as twin-peak HF QPOs and provide valuable information on infalling matter in the environment surrounding the compact object. Note that the latter can be changed in frequency as compared to the HF QPOs, which do not tend to drift in frequency (Tasheva & Stefanov 2019). Recent astrophysical observations suggest that LF and HF QPOs arise in separate parts of an accretion disk (Titarchuk & Shaposhnikov 2005; Stuchlik et al. 2007; Aliev et al. 2013; Dokuchaev & Eroshenko 2015; Kološ et al. 2015; Germanà 2018; Azreg-Aïnou et al. 2020; Ghasemi-Nodehi et al. 2020; Jusufi et al. 2021; Rayimbaev et al. 2021, 2022; Tarnopolski & Marchenko 2021), but both would be created together in some X-ray binary systems. Different models also

explain the appearance of HF QPOs in accretion disks (Stella et al. 1999; Rezzolla et al. 2003; Török et al. 2005; Páris et al. 2019; Shaymatov et al. 2020; Tursunov et al. 2020).

In order to test and compare the properties of the extended gravity theories, one may use a parameterization that would be able to mimic various gravity theories through an expansion of the metric functions in infinitely small dimensionless parameters. A first astrophysically interesting perturbative approach based on a perturbations on  $M/r$  as deviations of the Kerr metric was developed in Johannsen & Psaltis (2011) and Glampedakis et al. (2017). A new parameterization as an expansion in small dimensionless distance from the event horizon was developed for a spherically symmetric PRZ metric (Rezzolla & Zhidenko 2014) and was later extended for an axially symmetric metric by Konoplya–Rezzolla–Zhidenko (KRZ; Konoplya et al. 2016).

In this paper, the main idea is to constrain the first two expansion parameters of the PRZ parameterization with the help of the classical SS tests, the data of the S2 star orbiting the Sgr A\*, and the observed frequencies of the QPOs for the selected microquasars. By comparing the theoretical results with observations in the SS, the S2 star, and astrophysical quasiperiodic oscillations observed in GRO J1655-40 and XTE J1550-564 microquasars, we can provide the magnitude of these parameter constraints. Our investigation gives rise to the fact that the constraints provide much information to reveal the properties of this spacetime near the horizon, and they can be regarded as a powerful tool in the direction of mimicking the spherically symmetric and slowly rotating black holes.

The outline of the paper is as follows. In Section 2 we study the geodesics of time-like test particles in the background determined by the spherically symmetric PRZ spacetime (Rezzolla & Zhidenko 2014). In Section 3.1 we study and derive the expression for the perihelion shift with the aim to obtain the constraints on the first two expansion parameters by comparing observational data. Sections 3.2 and 3.3 are devoted to discussing light bending and gravitational time delay. In Section 4 we discuss constraints on the expansion parameters of spherically symmetric PRZ spacetime via the S2 star orbit data. We further study the epicyclic motions and aim to constrain the expansion parameters by applying them to the QPOs observed in microquasars in Section 5. The concluding remarks are given in Section 6.

We use a system of units in this paper in which  $G_N = \hbar = c = 1$  (however, for expressions with an astrophysical application, we have written the speed of light and Newtonian gravitational constant explicitly), and is a spacetime signature  $(-, +, +, +)$ .

## 2. Spherically Symmetric PRZ Spacetime

The line element describing any spherically symmetric spacetime in the Schwarzschild coordinates  $(t, r, \theta, \phi)$  is given by Rezzolla & Zhidenko (2014),

$$\begin{aligned} ds^2 &= -g_t(r)dt^2 + g_r(r)dr^2 + g_{\theta\theta}(r)d\Omega^2 \\ &= -N^2(r)dt^2 + \frac{B^2(r)}{N^2(r)}dr^2 + r^2d\Omega^2, \end{aligned} \quad (1)$$

where  $d\Omega^2 \equiv d\theta^2 + \sin^2\theta d\phi^2$ , and  $N$  and  $B$  are functions of the radial coordinate  $r$  only with

$$N(r_0) = 0. \quad (2)$$

Note here that we omit any cosmological effect for the line element in Equation (1) to be an asymptotically flat spacetime

from its asymptotic properties. Following PRZ (Rezzolla & Zhidenko 2014), we introduce the following dimensionless variable for the radial coordinate:

$$x \equiv 1 - \frac{r_0}{r}, \quad (3)$$

where  $x = 0$  and  $x = 1$  correspond to the location of the event horizon  $r = r_0$  and to spatial infinity  $r = \infty$ , respectively. Taking into account the above dimensionless variable, we can rewrite the function  $N$  as follows:

$$N^2 = xA(x), \quad (4)$$

with  $A(x) > 0$  for  $0 \leq x \leq 1$ . Let us then write the functions  $A$  and  $B$  in terms of three additional parameters,  $\epsilon$ ,  $a_0$ , and  $b_0$ , i.e.,

$$\begin{aligned} A(x) &= 1 - \epsilon(1 - x) + (a_0 - \epsilon)(1 - x)^2 + \tilde{A}(x)(1 - x)^3, \\ B(x) &= 1 + b_0(1 - x) + \tilde{B}(x)(1 - x)^2, \end{aligned} \quad (5)$$

with the functions  $\tilde{A}(x)$  and  $\tilde{B}(x)$ ,

$$\tilde{A}(x) = \frac{a_1}{1 + \frac{a_2 x}{1 + \frac{a_3 x}{1 + \dots}}}, \quad (6)$$

$$\tilde{B}(x) = \frac{b_1}{1 + \frac{b_2 x}{1 + \frac{b_3 x}{1 + \dots}}}, \quad (7)$$

which are proposed to introduce the spacetime at the horizon,  $x \simeq 0$ , and at the spatial infinity,  $x \simeq 1$ . Note that  $a_1, a_2, a_3 \dots$  and  $b_1, b_2, b_3 \dots$  are the dimensionless constants in the above equations. It is possible for these constants to be constrained on the basis of astronomical observations near the event horizon. Furthermore, we obtain the constraints on the first two expansion parameters by using observational data. From the properties of expansions (6) and (7), the first two terms at the horizon can be written as

$$\tilde{A}(0) = a_1, \quad \tilde{B}(0) = b_1. \quad (8)$$

Therefore, the lowest-order terms would have primary importance near the horizon. Here, we introduce the new additional parameters  $\alpha$  and  $\lambda$  to describe only the lowest-order terms up to  $a_1$  and  $b_1$  near the horizon, so that the functions  $\tilde{A}(x)$  and  $\tilde{B}(x)$  can be expressed as follows:

$$\begin{aligned} xA(x) &= 1 - (1 + \epsilon)(1 - x) + a_0(1 - x)^2 \\ &+ (a_1 - a_0 + \epsilon)(1 - x)^3 - a_1(1 - x)^4, \end{aligned} \quad (9)$$

$$\begin{aligned} \frac{B^2(x)}{N^2(x)} &= 1 + (1 + \epsilon + 2b_0)(1 - x) \\ &+ (2b_1 + 2b_0(1 + \epsilon) - a_0)(1 - x)^2. \end{aligned} \quad (10)$$

### 2.1. PPN Formalism

An interesting advantage of the PPN formalism is that it constrains many theories of gravity. Here, we can specifically add the new parameters along with the PPN asymptotic

behavior by representing  $B$  and  $N$  as

$$\begin{aligned} N^2 &= 1 - \frac{2M}{r} + (\beta - \gamma) \frac{2M^2}{r^2} + \alpha \frac{2M^3}{r^3} + \mathcal{O}(r^{-4}) \\ &= 1 - \frac{2M}{r_0}(1 - x) + (\beta - \gamma) \frac{2M^2}{r_0^2}(1 - x)^2 \\ &+ \alpha \frac{2M^3}{r_0^3}(1 - x)^3 + \mathcal{O}((1 - x)^4), \end{aligned} \quad (11)$$

$$\begin{aligned} \frac{B^2}{N^2} &= 1 + \gamma \frac{2M}{r} + \lambda \frac{2M^2}{r^2} + \mathcal{O}(r^{-2}) \\ &= 1 + \gamma \frac{2M}{r_0}(1 - x) + \lambda \frac{2M^2}{r_0^2}(1 - x)^2 + \mathcal{O}((1 - x)^3), \end{aligned} \quad (12)$$

where  $M$  is the Arnowitt–Deser–Misner (ADM) mass of the spacetime parameters,  $\beta$  and  $\gamma$  are the PPN parameters, which are observationally constrained to be (Will 2006)

$$|\beta - 1| \lesssim 2.3 \times 10^{-4}, \quad |\gamma - 1| \lesssim 2.3 \times 10^{-5}, \quad (13)$$

while  $\alpha$  and  $\lambda$  are new dimensionless parameters related to the new coefficients  $a_1$  and  $b_1$ , respectively.

We have expanded the metric function  $N(r)$  to  $\mathcal{O}((1 - x)^4)$ , but kept  $B^2(r)/N^2(r)$  to  $\mathcal{O}((1 - x)^3)$  as the highest-order constraint on  $N(r)$  and  $B^2(r)/N^2(r)$  that allowed us to find the parameters  $\alpha$  and  $\lambda$ . So that the parameter  $\alpha$  sets constraint on  $N(r)$  to third order, while  $\lambda$  sets a constraint on  $B^2(r)/N^2(r)$  to second order in  $(1 - x)$ . By comparing the two asymptotic expansions (9)–(10) and (11)–(12), and collecting terms at the same order, we find that

$$1 + \epsilon = \frac{2M}{r_0}, \quad (14)$$

$$a_0 = (\beta - \gamma) \frac{2M^2}{r_0^2}, \quad (15)$$

$$1 + \epsilon + 2b_0 = \gamma \frac{2M}{r_0}, \quad (16)$$

$$a_1 + \epsilon - a_0 = \alpha \frac{2M^3}{r_0^3}, \quad (17)$$

$$2b_1 + 2b_0(1 + \epsilon) - a_0 = \lambda \frac{2M^2}{r_0^2}. \quad (18)$$

Hence, the introduced dimensionless constant  $\epsilon$  is completely fixed by the horizon radius  $r_0$  and the ADM mass  $M$  as

$$\epsilon = \frac{2M - r_0}{r_0} = - \left( 1 - \frac{2M}{r_0} \right), \quad (19)$$

and thus, it measures the deviations of  $r_0$  from  $2M$ . On the other hand, the coefficients  $a_0, b_0, a_1$ , and  $b_1$  can be seen as combinations of the PPN parameters and the new parameters  $\lambda$

and  $\alpha$  as

$$\begin{aligned} a_0 &= \frac{(\beta - \gamma)(1 + \epsilon)^2}{2}, \\ b_0 &= \frac{(\gamma - 1)(1 + \epsilon)}{2}, \\ a_1 &= \left[ \beta - \gamma + \frac{\alpha(1 + \epsilon)}{2} \right] \frac{(1 + \epsilon)^2}{2} - \epsilon, \\ b_1 &= \left[ \frac{\lambda}{2} - 2(\gamma - 1) + \frac{\beta - \gamma}{2} \right] \frac{(1 + \epsilon)^2}{2}, \end{aligned} \quad (20)$$

alternatively, as

$$\beta = 1 + \frac{2[a_0 + b_0(1 + \epsilon)]}{(1 + \epsilon)^2}, \quad (21)$$

$$\gamma = 1 + \frac{2b_0}{1 + \epsilon}. \quad (22)$$

Hereafter, we study the motion of test particles in the PRZ spacetime of Equation (1) so as to determine constraints of the parameters with the help of SS effects. Note that the PRZ black hole spacetime, being static and spherically symmetric, admits two Killing vectors, i.e.,  $\xi_{(t)}^\mu = (\partial/\partial t)^\mu$  and  $\xi_{(\phi)}^\mu = (\partial/\partial \phi)^\mu$ , which are referred to as stationary and an axisymmetry. Hence, there exist two conserved quantities, i.e., the energy  $E$  and the angular momentum  $l$  of the massive particle. Following these two Killing vectors, one can write the generalized momenta as follows:

$$-E = g_{\mu\nu} u^\mu \xi_{(t)}^\nu = -N^2(r) \dot{t}, \quad (23)$$

$$l = g_{\mu\nu} u^\mu \xi_{(\phi)}^\nu = \frac{B^2(r)}{N^2(r)} \dot{\phi}, \quad (24)$$

where  $u^\mu = \frac{dx^\mu}{d\tau}$  refers to the four-velocity of the massive particle with the coordinate four-vector  $x^\mu$ , and the dot denotes the derivative with respect to the proper time  $\tau$  of a massive particle. Solving the above equations would give the equations of motion for a massive particle. Note that we furthermore restrict the motion to the equatorial plane, i.e.,  $\theta = \pi/2$ . The equation of motion of the massive particle can then be written as

$$\dot{t} = \frac{E}{N^2(r)} \text{ and } \dot{\phi} = \frac{N^2(r)}{B^2(r)} l, \quad (25)$$

with the one given in terms of the effective potential as

$$\frac{\dot{r}^2}{2} + V^{\text{eff}} = E^2, \quad (26)$$

where we defined that  $E = E/m$  and  $l = l/m$  are conserved quantities. Taking all together, the effective potential for time-like massive particles reads

$$\begin{aligned} V^{\text{eff}} &= -\frac{M}{r} - (2 - \beta - \gamma) \frac{M^2}{r^2} + \frac{l^2}{2r^2} \\ &\times \left[ 1 - \gamma \frac{2M}{r} - (\lambda - 2\gamma^2) \frac{2M^2}{r^2} \right] \\ &- (4 - 4\beta + 2\beta\gamma + 2\gamma^2 - 2\lambda - \alpha) \frac{M^3}{r^3}. \end{aligned} \quad (27)$$

For light-like test particles, the effective potential simplifies to

$$\begin{aligned} V^{\text{eff}} &= -(1 - \gamma) \frac{M}{r} - (2 - \beta - \gamma - \lambda + 2\gamma^2) \frac{M^2}{r^2} \\ &+ \frac{l^2}{2r^2} \left[ 1 - \gamma \frac{2M}{r} - (\lambda - 2\gamma^2) \frac{2M^2}{r^2} \right] \\ &- (4 - 4\beta + 2\beta\gamma + 2\gamma^2 - 2\lambda - \alpha) \frac{M^3}{r^3}. \end{aligned} \quad (28)$$

The first term of expression (27) is the Newton potential, whereas the second and third terms correspond to the centrifugal barrier and relativistic correction relevant to the parameters of spherically symmetric PRZ spacetime (Rezzolla & Zhidenko 2014). The effective potentials are essential for the SS effects in order to find constraints on the parameters from observational data.

### 3. Limits on the Parameters of the PRZ Spacetime via SS Tests

#### 3.1. Perihelion Shift

In this subsection, we aim to derive the analytic form of the perihelion shift in the case of low eccentricity and small expansion parameters (Wald 1984). Particles will oscillate harmonically around some stable circular orbit at radius  $r = r_+$  with a frequency that is given by

$$\begin{aligned} \omega_r^2 &= \frac{1}{r_+^2} \left\{ -\frac{2M}{r_+} + \frac{l^2}{r_+^2} \left[ 3 - 12\gamma \frac{M}{r_+} - 20(\lambda - 2\gamma^2) \frac{M^2}{r_+^2} \right] \right. \\ &- (2 - \beta - \gamma) \frac{6M^2}{r_+^2} \\ &\left. - (4 - 4\beta + 2\beta\gamma - 2\lambda - \alpha) \frac{12M^3}{r_+^3} \right\}. \end{aligned} \quad (29)$$

The condition  $dV^{\text{eff}}/dr|_{r=r_+} = 0$  allows one to determine the angular momentum and the angular frequency  $\omega_\phi = |l|/r_+^2$ , where  $l$  is the conserved angular momentum, which then takes the form

$$\begin{aligned} \omega_\phi^2 &= \frac{r_+^{-2}}{1 - 3\gamma \frac{M}{r_+} - 4(\lambda - 2\gamma^2) \frac{M^2}{r_+^2}} \\ &\times \left[ \frac{M}{r_+} + (2 - \beta - \gamma) \frac{2M^2}{r_+^2} \right. \\ &\left. + (4 - 4\beta + 2\beta\gamma - 2\lambda - \alpha) \frac{3M^3}{r_+^3} \right]. \end{aligned} \quad (30)$$

The perihelion precession is given by

$$\begin{aligned} \omega_p &= \frac{3M^{3/2}}{r_+^{5/2}} \left\{ 1 + \frac{2\gamma - \beta - 1}{3} + \frac{1}{6} \frac{M}{r_+} \right. \\ &\times \left[ 6(A_1 + 2\lambda) - A_2^2 + 9A_2\gamma - 6\gamma^2 \right] + O\left(\frac{1}{r_+^2}\right) \left. \right\}, \end{aligned} \quad (31)$$

where  $A_1 = 4 - 4\beta + 2\beta\gamma + 2\gamma^2 + 2\lambda - \alpha$  and  $A_2 = 2 - \beta - \gamma$ . Following Weinberg (1972), the perihelion precession in the above equation can be written in terms of the finite eccentricity

**Table 1**

Numerical Values of the Semimajor Axes  $P$ , the Eccentricities  $e$ , the Perihelion Shifts  $\Delta\phi$ , and the Relative Perihelion Shifts  $\delta\omega_p/\omega_p$  Tabulated for All SS Planets (Carloni et al. 2011)

Planet	Mercury	Venus	Earth	Mars	Jupiter	Saturn	Uranus	Neptune	Icarus
$P$	$4 \cdot 10^{45}$	$7 \cdot 10^{45}$	$9 \cdot 10^{45}$	$1.4 \cdot 10^{46}$	$5 \cdot 10^{46}$	$9 \cdot 10^{46}$	$1.8 \cdot 10^{47}$	$3 \cdot 10^{47}$	$1.0 \cdot 10^{46}$
$e$	0.2	0.007	0.017	0.09	0.05	0.06	0.05	0.011	0.8
$\Delta\phi = 2\pi\omega_p P^{3/2}/\sqrt{M}$	43	8.6	3.8	1.3	0.06	0.014	0.002	0.0007	9.8
$\delta\omega_p/\omega_p$	$1.2 \cdot 10^{-4}$	$3 \cdot 10^{-2}$	$1.1 \cdot 10^{-4}$	$4 \cdot 10^{-4}$	0.6	$3 \cdot 10^2$	$7 \cdot 10^3$	?	$8 \cdot 10^{-2}$

**Note.** We note, however, that the values of the uncertainties in the perihelion shifts of SS planets have been discussed and presented recently in Iorio (2015, 2019).

and the semimajor axis as follows:

$$\omega_p = \frac{3M^{3/2}}{(1-e^2)P^{5/2}} \left\{ 1 + \frac{2\gamma - \beta - 1}{3} + \frac{1}{6} \frac{M}{r_+} \right. \\ \left. \times \left[ 6(A_1 + 2\lambda) - A_2^2 + 9A_2\gamma - 6\gamma^2 \right] + O\left(\frac{1}{r_+^2}\right) \right\}, \quad (32)$$

where  $P$  and  $e$  refer to the semimajor axis and eccentricity of the ellipse, respectively. After some straightforward calculations, we obtain the perihelion shift as follows:

$$\Delta\phi = \frac{6\pi M}{(1-e^2)P} \left\{ 1 + \frac{2\gamma - \beta - 1}{3} + \frac{1}{6} \frac{M}{r_+} \right. \\ \left. \times \left[ 6(A_1 + 2\lambda) - A_2^2 + 9A_2\gamma - 6\gamma^2 \right] + O\left(\frac{1}{r_+^2}\right) \right\}, \quad (33)$$

where the leading-order term in Equation (33) must be small so that it does not conflict with observational data. Considering now the observational data (Carloni et al. 2011) tabulated in Table 1 and using the PPN bound, we try to gauge the value of the residual perihelion shifts of the planet Mercury  $\delta\omega_p/\omega_p$  in particular cases. With the solar mass given by  $M \approx 9 \cdot 10^{37}$  in Planck units, the third term of the expression in Equation (33) is extremely small,

$$\frac{M}{r_+}(4\lambda - \alpha) \ll 1, \quad (34)$$

because  $M/r_+ \sim M/P \approx 10^{-8}$ . For this, the perihelion shift data become very weak and do not allow one to derive strong constraints on the value of the expansion parameters  $\lambda$  and  $\alpha$  together with the PPN parameters. Hence, the bound from the perihelion shift cannot give strong constraints on the abovementioned parameters. Furthermore, Equation (34) implies that

$$\lambda \ll 1 \text{ and } \alpha \ll 1. \quad (35)$$

### 3.2. Light Bending

In this subsection, we study and explore the classical light bending. To do this, we consider the quantity  $\dot{r}$  in Equation (26), which vanishes at the point where the worldline of the photon becomes close to the Sun, i.e.,  $r = r_0$ . Thus, the effective potential given by Equation (28) is taken to be the energy  $E$  at  $r_0$ . Placing

this value for  $E$  into Equation (26) with the photon trajectory, one can then have the following expression:

$$\frac{dr}{d\phi} = \frac{rN(r)}{B(r)} \left[ \left( \frac{rN(r_0)}{r_0N(r)} \right)^2 - 1 \right]^{1/2}, \quad (36)$$

where the  $N(r)$  and  $B(r)$  functions are given in Equation (11). Now it is straightforward to obtain the photon deflection angle as follows:

$$\Delta\varphi = 2 \int_{r_0}^{\infty} \frac{dr}{\frac{rN(r)}{B(r)} \left[ \left( \frac{rN(r_0)}{r_0N(r)} \right)^2 - 1 \right]^{1/2}} - \pi \\ = \frac{4M}{r_0} \left\{ \frac{1+\gamma}{2} - \gamma \frac{M^2}{r_0^2} + \frac{(3\gamma-\beta)M^2}{4r_0^2} \pi + \frac{\lambda M^2}{8r_0^2} \pi \right. \\ \left. - \left[ \gamma(\beta-\gamma) + \alpha + \frac{\alpha}{4} \pi \right] \frac{M^3}{2r_0^3} + O\left(\frac{M}{r_0}\right)^4 \right\} \\ = \frac{4M}{r_0} \left( \frac{1+\gamma}{2} \right) + \delta\Delta\varphi. \quad (37)$$

Here we note that the term  $4M/r_0$  refers to the general relativistic effect, and the rest of all terms in brackets in Equation (37) must be sufficiently small to avoid conflicting with observational data. Now we take into account the observational data for the deflection angle (Shapiro et al. 2004; Carloni et al. 2011), which allows one to constrain the expansion parameters  $\lambda$  and  $\alpha$  through the bound on the deflection angle,

$$-1.2 \times 10^{-3} < \frac{\delta\Delta\varphi}{\Delta\varphi} < 4 \times 10^{-4}. \quad (38)$$

The term  $\delta\Delta\varphi$  in the above expression includes the second- and third-order terms in  $M/r_0$ . Following Carloni et al. (2011),  $r_0$  can approximately be taken to be two solar radii, i.e.,  $r_0 \approx 8 \times 10^{43}$  in Planck units. Plugging this value into Equation (38), one can constrain the expansion parameters  $\alpha$  and  $\lambda$ . However, it turns out to be very complicated to obtain the constraints on these parameters because  $\delta\Delta\varphi$  includes higher-order terms of  $M/r_0$  that could be equal to a very low value, which is of order  $(M/r_0)^2 \approx 10^{-12}$  and  $(M/r_0)^3 \approx 10^{-18}$ . It does therefore turn out that the deflection angle with the observational data cannot provide strong constraints on the abovementioned parameters. One can expect, however, that these parameters take low values, i.e.,  $\lambda \sim \alpha \ll 1$ .

### 3.3. Radar Echo Delay

We then turn to the standard measurement of the time delay that stems from the light bending. Here, we consider the time delay of light and evaluate it together with clock effects for a radar signal that is sent from Earth to some object and is reflected back from the target to Earth (see, e.g., Weinberg 1972). To do this, we first consider the following differential equation, which can be written as follows:

$$\frac{dr}{dt} = \frac{N^2(r)}{B(r)} \left[ 1 - \left( \frac{N(r)r_0}{N(r_0)r} \right) \right]^{1/2}. \quad (39)$$

From this equation, we calculate the integral for the time in which the light travels from  $r_0$  to  $r$ . Hence, it has the form

$$\begin{aligned} t(r, r_0) = & \int_{r_0}^r \left( 1 - \frac{r_0^2}{r^2} \right)^{-1/2} \left\{ 1 + (1 + \gamma) \frac{M}{r} \right. \\ & + \frac{Mr_0}{r(r + r_0)} + (4\gamma - 2\beta + \lambda) \frac{M^2}{r^2} \\ & + [2\lambda - 2\gamma(\beta - \gamma) - 2\alpha - 2(\gamma + 1)(\beta - \gamma)] \\ & \left. \times \frac{M^3}{r^3} - \alpha \frac{M^3}{r_0 r^2} + \alpha \frac{M^3}{r^2(r + r_0)} \right\} dr, \end{aligned} \quad (40)$$

and we then find the time delay in the general form as follows:

$$\begin{aligned} \Delta t = & 2 \left[ t(r_E, r_0) + t(r_T, r_0) - \sqrt{r_E^2 - r_0^2} - \sqrt{r_T^2 - r_0^2} \right] \\ = & 4M \left\{ 1 + \frac{1 + \gamma}{2} \ln \frac{4r_E r_T}{r_0^2} + (4\gamma - 2\beta + \lambda) \frac{M}{4r_0} \pi \right. \\ & + [\lambda - \gamma(\beta - \gamma) - 2\alpha - (\gamma + 1)(\beta - \gamma)] \\ & \left. \times \frac{M^2}{r_0^2} + O\left(\frac{M}{r_0}\right)^3 \right\} \\ = & 4M \left( 1 + \frac{1 + \gamma}{2} \ln \frac{4r_E r_T}{r_0^2} \right) + \delta \Delta t. \end{aligned} \quad (41)$$

It is worth noting here that for the further analysis, we consider  $r_0$  as a distance that is on the order of the solar radius. Also,  $r_T$  and  $r_E$  refer to the distance of the target and of the Earth, respectively, from the Sun. However, we consider for simplicity  $r_T$  and  $r_E$  as the semimajor axes of the orbits of the target and the Earth for the further analysis (see Table 1). We note that in Equation (41), the first term on the right-hand side corresponds to the general relativistic PPN result, while the second term corresponds to the correction that comes from the expansion parameters of spherically symmetric PRZ spacetime. In doing this, we analyze the time delay and its bound in order to obtain both upper and lower limits on the expansion parameters  $\lambda$  and  $\alpha$  using the observational data (Bertotti et al. 2003),

$$-10^{-6} < \frac{\delta \Delta t}{\Delta t} < 2 \cdot 10^{-5}, \quad (42)$$

which in turn allows one to determine the bound for higher-order expansion parameters associated with the higher-order terms of  $M/r_0$ . However,  $M^2/r_0^2$  in the third term of Equation (41) is  $\approx 10^{-12}$  when the distance is taken to be  $r_0 \approx 7 \times 10^{43}$  (see, e.g., Bertotti et al. 2003). It therefore does not cause explicit constraints on these higher-order expansion parameters. As a consequence of the analysis of the time delay due to light bending, one can deduce that these higher-order expansion parameters could take low values, i.e.,  $\lambda \sim \alpha \ll 1$ , similarly to what was observed in the previous analysis.

In this section, we have shown that it is not possible to obtain accurate and explicit constraints on the higher-order expansion parameters  $\alpha$  and  $\lambda$  through the observational data for the solar system tests because the factors  $M/r_+$  and  $M/r_0$  and their higher-order terms in the expression of perihelion shift, light deflection and gravitational time delay, are infinitely small and thus have no significant impact on SS tests. Therefore, the capacity of the observational data for SS tests is not high enough to place a strong constraint on the higher-order expansion parameters of the PRZ spacetime. To obtain the best-fit constraints on these expansion parameters, we must test and consider observations of phenomena of the S2 star, which is located in the star cluster close to Sgr A\*. It would therefore be expected that the observational data for the S2 star orbiting Sgr A\* are capable to constrain the higher-order expansion parameters. This is what we intend to examine in the next section.

## 4. Limits on the Parameters of the PRZ Spacetime via the Orbit Data of Star S2

The Galactic center of the Milky Way galaxy provides an excellent physics laboratory for various observational and experimental tests of the black hole models and theories of modified gravity in their most extreme limits. In fact, it was argued that one can use the S cluster stars to set constraints on the black hole mass, which is  $4.07 \times 10^6 M_\odot$  at a distance of approximately 8.35 kpc from us (Gillessen et al. 2017). So far, there is no observational evidence that Sgr A\* possesses an astrophysical jet or any accretion disk. Moreover, it is less clear whether Sgr A\* is accreting gas via Bondi radially infall accretion or through a disk. However, the indirect evidence of an accretion disk about Sgr A\* is relevant to the recent detection of the Sgr A\* shadow reported by the Event Horizon Telescope (EHT) collaboration (Akiyama et al. 2022). The shadow is formed by the light emitted from the accretion disk, which subsequently is deflected by the black hole and eventually arrives at the EHT detectors. Further constraints on the mass, spin, and geometry of the Sgr A\* black hole can be deduced from the observations of its shadow in the near future (Perlick & Tsupko 2022).

In this section, we focus on the constraints of the expansion parameters by using observations of phenomena of star S2, which is located in the star cluster close to Sgr A\*. Star S2 orbits Sgr A\* (Ghez et al. 2000, 2005; Nucita et al. 2007; Lacroix 2018), and thus it plays an important role in a study of the physical properties of the central black hole, Sgr A\*, i.e., its parameters are of the primary astrophysical importance. It has very recently been shown that wormhole models as candidates for Sgr A\* are tested by the motion of the S2 star (see, e.g., Jusufi et al. 2022b). Moreover, the motion of star S2 has been

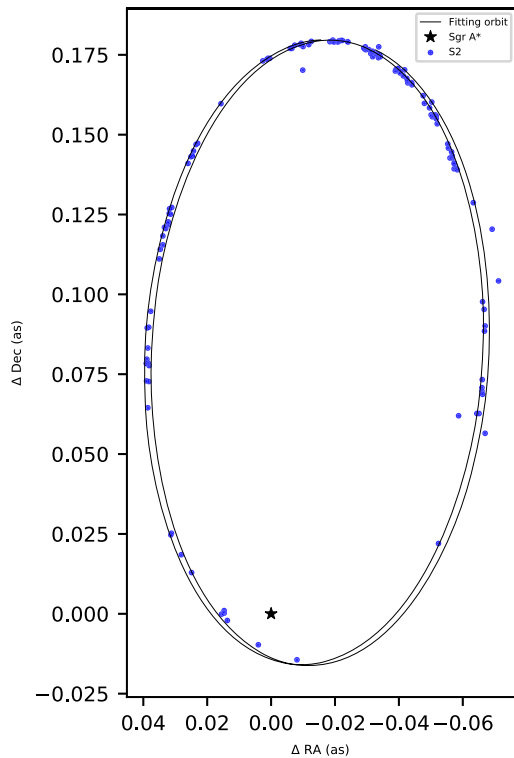


**Figure 1.** Observed orbit of star S2 around Sgr A\*. Note that we obtained the orbit of star S2 around Sgr A\* as a model fitting with PRZ spacetime geometry by applying the observational data.

used to constrain different models for the dark matter distribution inside the inner Galactic region, such as the dark matter spike model (Nampalliwar et al. 2021) or the loop quantum gravity model (Yan et al. 2022). Moreover, the S2 star observations have been used to constrain the barrow entropy (Jusufi et al. 2022a). With this motivation, we also consider the motion of the S2 star to set constraints on the parameters of PRZ black hole spacetime, as described by the line element proposed in Rezzolla & Zhidenko (2014), as a candidate for the Sgr A\* compact object at the center of the Milky Way galaxy.

Thus, we further consider the motion of star S2 around the PRZ spacetime geometry and solve the equations of motion numerically (see Becerra-Vergara et al. 2020 for details) by adapting the method related to the analysis of the periastron shift of the S2 star possessing orbit parameters. Thus, we limit the values of the expansion parameters of spherically symmetric PRZ spacetime through the phenomena of star S2. In Figure 1 we show the best-fitting orbit of star S2 as stated by the observational data given in Do et al. (2019). Note that the black five-pointed star polygon in Figure 1 indicates the location of Sgr A\*.

#### 4.1. Datasets

We further apply the astrometric and spectroscopic data for star S2. We note that these data are publicly available and have been collected. There are three various parts for these data: astrometric positions, radial velocities, and the pericenter precession, which we further use for our purpose. The details of these three parts can be summarized as follows: 1. *Astrometric positions*: 145 astrometric positions for star S2 starting from 1992.224 to 2016.53 as reported in

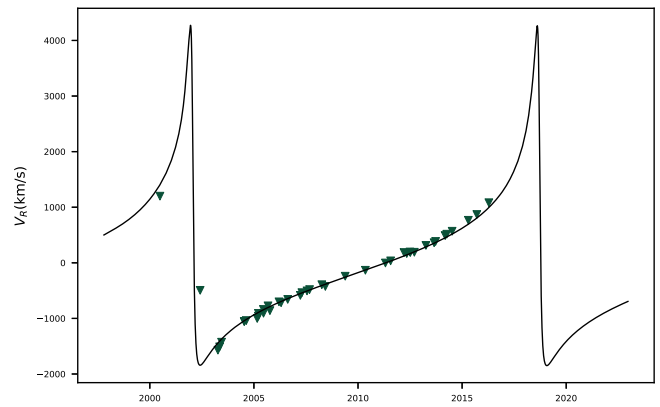


**Figure 2.** The dataset of the radial velocities of star S2 used in our analysis and the fitting curve by PRZ spacetime.

Gillessen et al. (2017) are used in our analysis. It is worth noting that before 2002, all data were obtained/collected from the ESO New Technology Telescope (NTT), while the remaining data were collected since 2002 from the Very Large Telescope (VLT). In Figure 1 we plot these data. We show the data from NTT and VLT as blue and red points, respectively, as shown in Figure 1. 2. *Radial velocities*: the data for 44 radial velocities can be used from 2000.487 to 2016.519 (see, e.g., Gillessen et al. 2017). Similarly, the data for the radial velocities were collected by various observing sources, i.e., the data from NIRC2 before 2003 and from the INtegral Field Observations in the Near Infrared (SINFONI) after 2003. We show these data in Figure 2 for the radial velocity  $V_R$  as a function of epoch year. 3. *Orbital precession of star S2*: the orbital precession of star S2 has been observed and measured by the GRAVITY Collaboration (see, e.g., GRAVITY Collaboration 2020),

$$\Delta\phi_{\text{per orbit}} = 1.10 \pm 0.19. \quad (43)$$

It is a well-known fact that the orbital precession becomes an important phenomenon as a remarkable prediction of GR (see Figure 1). For our purpose, we apply its measurement in the analysis of the Markov Chain Monte Carlo (MCMC) simulations.

#### 4.2. Modeling the Orbit with Relativistic Effects

We consider the equations of motion for massive particles and apply them to explore the motion of the orbit of star S2 with relativistic effects. To do this, one needs to integrate Equations (25) and (26) numerically by imposing the initial conditions, including coordinates  $\{t(\lambda_0), r(\lambda_0), \phi(\lambda_0)\}$ , and their first derivatives  $\{\dot{t}(\lambda_0), \dot{r}(\lambda_0), \dot{\phi}(\lambda_0)\}$ . This would play a key role in deriving the positions of star S2 in the orbital plane, but its astrometric positions as stated above can be determined in the celestial plane. The point to be noted here is that one can approximate the motion of star S2 in the abovementioned two planes by using the elliptical orbit. It is then possible to compare the theoretical and astrometric positions if and only if one considers all observational quantities to lie in the same plane. For this purpose, one can consider a projection of the theoretical positions on the celestial plane with the help of the following coordinate transformations:

$$X = x\mathcal{B} + y\mathcal{G}, \quad (44)$$

$$Y = x\mathcal{A} + y\mathcal{F}, \quad (45)$$

$$Z = x\mathcal{C} + y\mathcal{H}. \quad (46)$$

Here, we note that  $(X, Y, Z)$  and  $(x, y, z)$  refer to the coordinates in the celestial and the orbital planes, respectively, while  $\mathcal{A}, \mathcal{B}, \mathcal{C}, \mathcal{F}, \mathcal{G}, \mathcal{H}$  are the corresponding coefficients, which are defined by

$$\mathcal{A} = \cos \Omega' \cos \omega' - \sin \Omega' \sin \omega' \cos i, \quad (47)$$

$$\mathcal{B} = \sin \Omega' \cos \omega' + \cos \Omega' \sin \omega' \cos i, \quad (48)$$

$$\mathcal{C} = \sin \omega' \sin i, \quad (49)$$

$$\mathcal{F} = -\cos \Omega' \sin \omega' - \sin \Omega' \cos \omega' \cos i, \quad (50)$$

$$\mathcal{G} = -\sin \Omega' \sin \omega' + \cos \Omega' \cos \omega' \cos i, \quad (51)$$

$$\mathcal{H} = \cos \omega' \sin i, \quad (52)$$

where  $\omega'$  and  $\Omega'$  refer to the perihelion argument and the longitude of ascending node, respectively, with the orbital inclination  $i$  of star S2 the elliptical orbit.

We furthermore assume that an offset exists between the gravitational center and the reference frame considered here, and thus we have  $x_0, y_0, v_{x0}$ , and  $v_{y0}$  for the further modeling process (see, e.g., Do et al. 2019),

$$X = X(t_{\text{em}}) + x_0 + v_{x0}(t_{\text{em}})(t_{\text{em}} - t_{\text{J2000}}), \quad (53)$$

$$Y = Y(t_{\text{em}}) + y_0 + v_{y0}(t_{\text{em}})(t_{\text{em}} - t_{\text{J2000}}). \quad (54)$$

Here we would like to mention that  $t_{\text{J2000}}$  and  $t_{\text{em}}$  are used to delineate the Julian year 2000 and the epoch of the emitting light, respectively. To compare these theoretical positions with the astrometric data, one also needs to take several relativistic effects into account.

We first take the Romer time delay effect into consideration because it changes the arrival time of the light that comes from the orbiting star located far way or closer to the Earth. We define the Romer time delay as follows:

$$t_{\text{obs}} - t_{\text{em}} = \frac{Z(t_{\text{em}})}{c}, \quad (55)$$

with the epoch  $t_{\text{obs}}$  when the light is observed, while  $Z$  is derived from Equations (46). However, it is very complicated to solve this equation, but an alternative method exists to approach and solve this equation (for details, see GRAVITY Collaboration 2018; Do et al. 2019), and it is given by

$$t_{\text{em}}^{(i+1)} = t_{\text{obs}} - \frac{Z(t_{\text{em}}^{(i)})}{c}. \quad (56)$$

After some iterations, this yields

$$t_{\text{em}} \approx t_{\text{obs}} - \frac{Z(t_{\text{obs}})}{c}. \quad (57)$$

Next, we wish to consider the effect of the frequency shift  $\zeta$  for a photon, which has the following relation associated with the radial velocity of star S2:

$$\zeta = \frac{\Delta\nu}{\nu} = \frac{\nu_{\text{em}} - \nu_{\text{obs}}}{\nu_{\text{obs}}} = \frac{V_{\text{R}}}{c}, \quad (58)$$

with the emitted frequency  $\nu_{\text{em}}$  and the observed frequency  $\nu_{\text{obs}}$  of the light, and the radial velocity  $V_{\text{R}}$  of star S2. Two main relativistic effects exist that can have a significant impact on the abovementioned frequency shift: the Doppler shift  $\zeta_{\text{D}}$ , and the effects of the gravitational redshift  $\zeta_{\text{G}}$ . For example, the first

effect we consider is the Doppler shift  $\zeta_{\text{D}}$ , which stems from the relative motion between the observer and the star. Thus, the Doppler shift can give rise to a significant impact such as that of the high orbital velocity of star S2,

$$\zeta_{\text{D}} = \frac{\sqrt{1 - \frac{v_{\text{em}}^2}{c^2}}}{1 - n \cdot v_{\text{em}}}. \quad (59)$$

Here, we note that  $v_{\text{em}}$  refers to the velocity measured at at  $t_{\text{em}}$ , while  $n \cdot v_{\text{em}}$  refers to the the projected velocity onto the light sight (i.e., the radial velocity). Another relativistic effect is the gravitational redshift  $\zeta_{\text{G}}$ , which is caused by a pure GR effect, and its frequency shift can be drastically influenced by a strong gravitational field,

$$\zeta_{\text{G}} = \frac{1}{\sqrt{-g_{tt}}}. \quad (60)$$

Because the frequency shift is relevant for the Doppler and gravitational field effects, it can then be defined by

$$\zeta = \zeta_{\text{D}} \cdot \zeta_{\text{G}} - 1. \quad (61)$$

We further need to describe the corresponding radial velocity  $V_{\text{R}}$  of star S2. For this purpose, we consider that any movement of Sgr A\* toward the Sun would lead to a change in the velocity, i.e, there may exist an offset and drift between the reference frame and the gravitational center. To model  $V_{\text{R}}$ , one needs to introduce a new parameter  $v_{z0}$ . One can then be able to define the radial velocity of the S2 star via  $v_{z0}$ , similarly to what was done previously for the positions given by Equations (44)–(46). Hence, it can be written as follows (Reid et al. 2007):

$$V_{\text{R}} = c \cdot \zeta + v_{z0}. \quad (62)$$

### 4.3. Analysis of the Markov Chain Monte Carlo

For the further analysis, we apply the MCMC simulations (see, e.g., Foreman-Mackey et al. 2013) in order to constrain the expansion parameters of spherically symmetric PRZ spacetime. Let us then introduce the set of parameters

$$\{M, R_0, a, e, i, \omega', \Omega', t_{\text{apo}}, x_0, y_0, v_{x0}, v_{y0}, v_{z0}, \beta, \gamma, \alpha, \lambda\}, \quad (63)$$

and explore them to obtained their best fit, with the available data associated with the theoretical orbits, as presented in Section 4.1. Here we note that  $M$  and  $R_0$  denote the black hole mass and the distance from the black hole to the Earth, respectively, while  $\{a, e, i, \omega', \Omega', t_{\text{apo}}\}$  represent the set of six orbital elements of the elliptical orbit of star S2, and another set of five parameters  $\{x_0, y_0, v_{x0}, v_{y0}, v_{z0}\}$  corresponds to the drifts of the reference frame and the zero-point offsets. The remaining four parameters  $\{\beta, \gamma, \alpha, \lambda\}$  are the expansion parameters of PRZ spacetime, as mentioned in the previous section. Another key point we note is that the orbit of star S2 may not be exactly an ellipse. However, we assume that the orbit is elliptical and refer to the osculating ellipse with the orbital elements mentioned above.

For the analysis of MCMC simulations together with the abovementioned parameter space, uniform priors were chosen



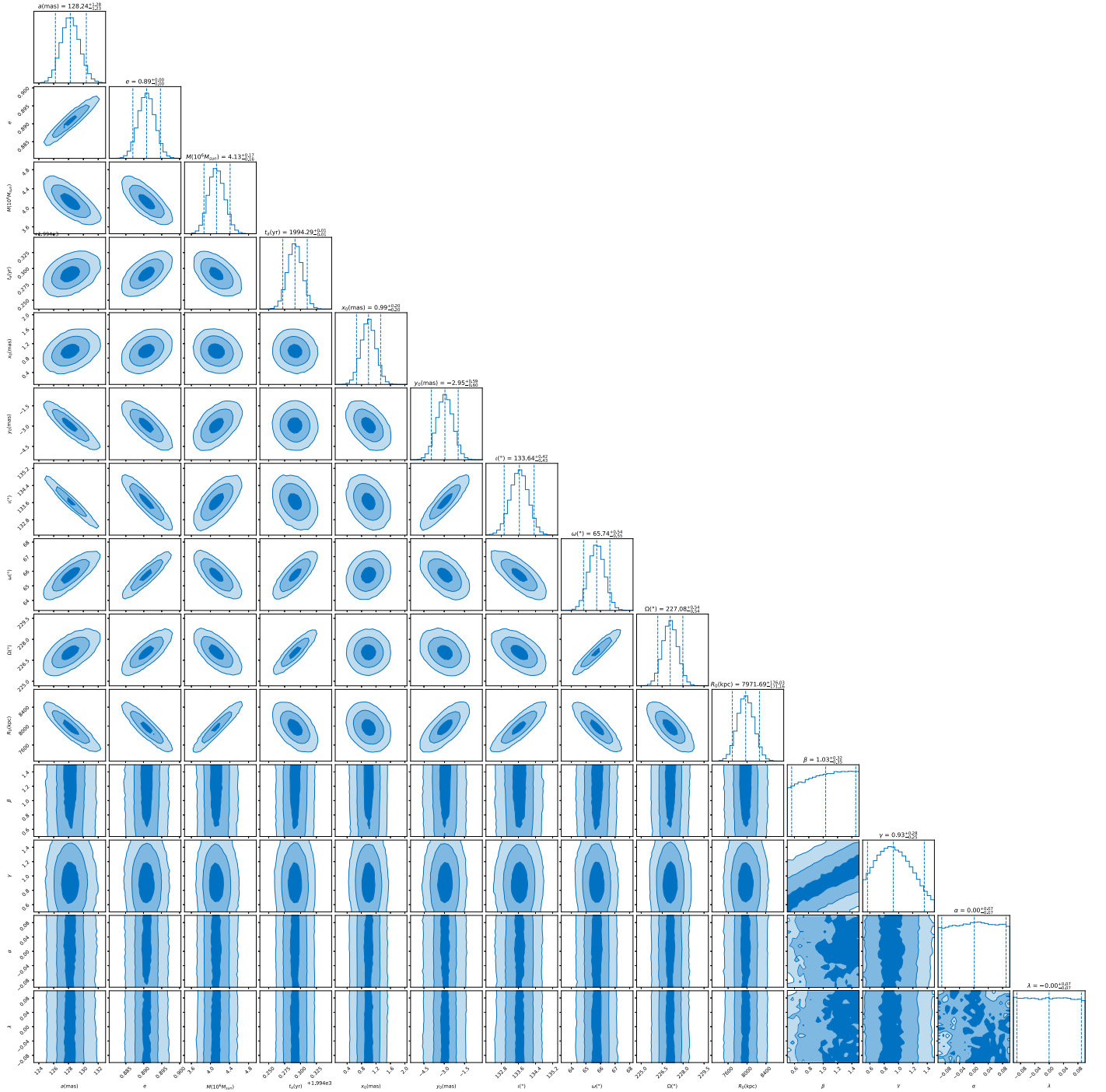


**Figure 3.** Posterior distribution of the orbital parameters of star S2 and the expansion parameters of PRZ spacetime associated with the uniform priors for these orbital parameters of star S2.

for all parameters. The ranges of parameters  $\beta$  and  $\gamma$  are set as  $[0, 2]$ , and the ranges of  $\{\alpha$  and  $\lambda\}$  are  $[-1, 1]$ .

It is worth noting here that three different parts of data exist, which, as mentioned in Section 4.1, can be applied to the analysis of the MCMC simulations. Hence, the probability function  $\mathcal{L}$  has three different parts, which are given by

$$\log \mathcal{L} = \log \mathcal{L}_{\text{AP}} + \log \mathcal{L}_{\text{VR}} + \log \mathcal{L}_{\text{pro}}, \quad (64)$$

where the first term,  $\log \mathcal{L}_{\text{AP}}$ , represents the probability of 145 astrometric positional data and is defined by

$$\log \mathcal{L}_{\text{AP}} = -\frac{1}{2} \sum_i \frac{(X_{\text{obs}}^i - X_{\text{the}}^i)^2}{(\sigma_{X,\text{obs}}^i)^2} - \frac{1}{2} \sum_i \frac{(Y_{\text{obs}}^i - Y_{\text{the}}^i)^2}{(\sigma_{Y,\text{obs}}^i)^2}, \quad (65)$$

**Table 2**

Constraint of the Best-fit Values of the Expansion Parameters  $\{\beta, \gamma, \alpha, \text{ and } \lambda\}$  and the Orbital Model Parameters of Star S2 in PRZ Spacetime Tabulated as Stated by the Analysis of the MCMC Simulations

Parameters	Best-fit Values
$M$ ( $10^6 M_\odot$ )	4.127
$R_0$ (kpc)	7971
$a$ (mas)	128.24
$e$	0.89077
$\iota$ ( $^\circ$ )	133.64
$\omega$ ( $^\circ$ )	65.741
$\Omega$ ( $^\circ$ )	227.07
$t_{\text{apo}}$ (yr)	1994.2913
$x_0$ (mas)	1.06
$y_0$ (mas)	-2.51
$v_{x0}$ (mas yr $^{-1}$ )	0.134
$v_{y0}$ (mas yr $^{-1}$ )	0.020
$v_{z0}$ (km s $^{-1}$ )	13.42
$\beta$	$1.03^{+0.32}_{-0.35}$
$\gamma$	$0.93^{+0.28}_{-0.25}$
$\alpha$	(-0.09, 0.09)
$\lambda$	(-0.09, 0.09)

**Note.** Note that the constraint ranges on the expansion parameters are obtained through the posterior region at the 90% confidence level.

and the second term,  $\log L_{\text{VR}}$ , describes the probability of 45 data for the radial velocities and reads

$$\log L_{\text{VR}} = -\frac{1}{2} \sum_i \frac{(V_{\text{R,obs}}^i - V_{\text{R,the}}^i)^2}{(\sigma_{V_{\text{R,obs}}}^i)^2}, \quad (66)$$

while the third term,  $\log \mathcal{L}_{\text{pro}}$ , represents the probability of the orbital precession and is given by

$$\log \mathcal{L}_{\text{pro}} = -\frac{1}{2} \frac{(\Delta\phi_{\text{obs}} - \Delta\phi_{\text{the}})^2}{\sigma_{\Delta\phi_{\text{obs}}}^2}, \quad (67)$$

where  $X_{\text{obs}}^i$ ,  $Y_{\text{obs}}^i$ , and  $V_{\text{R,obs}}^i$  refer to the data of the astrometric positions and radial velocities, respectively, and likewise  $X_{\text{the}}^i$ ,  $Y_{\text{the}}^i$ , and  $V_{\text{R,the}}^i$  refer to the theoretical predictions. Also,  $\sigma_{X_{\text{obs}}^i}$ , which appears in the above equation, refers to an appropriate statistical uncertainty for the corresponding quantities. Here, we would like to mention the orbital precession  $\Delta\phi_{\text{obs}}$  of star S2 given by Equation (43) and the theoretical one  $\Delta\phi_{\text{the}}$  given by Equation (33), involving the abovementioned expansion parameters of PRZ spacetime.

#### 4.4. Results and Discussions

Following all these subsections, we analyzed these 14-dimensional parameter spaces by adapting MCMC simulations and showing the posterior distributions of these parameter spaces for the orbital model of star S2 (see Figure 3). Note that we show the contour plots with 68%, 90%, and 95% confidence regions. The appropriate constraint values of these parameters are also tabulated in Table 2. This is particularly noteworthy because the results shown here in Figure 3 and Table 2 for the first two expansion parameters agree well with the results for PPN.

In Figure 3 we show the observational constraints on the expansion parameters of PRZ spacetime by using the data of

the orbital model of star S2. As a consequence of the analysis, as shown in Figure 3, we demonstrate the constraint values through the corresponding posterior distribution of the expansion parameters, so that the first two expansion parameters of PRZ spacetime are observationally constrained to be  $\beta = 1.03^{+0.32}_{-0.35}$  and  $\gamma = 0.93^{+0.28}_{-0.25}$  at the 90% confidence level. As stated above, these best-fit constraint values are completely consistent with the values for the PPN parameters, even though they are slightly stronger than those derived from observations of the solar system.

However, we find that the observational constraints of the higher-order expansion parameters,  $\alpha$ , and  $\lambda$ , through star S2 are more accurate than those of the SS test observations. This is because  $M/r_+$ , which appears in the third term of Equation (33), is  $\approx 10^{-4}$  for star S2, which orbits Sgr A\*, thus resulting in having a significant impact on the orbital parameters of star S2 as compared to the one for SS tests. Hence, we have shown that the observational data for S2 orbiting Sgr A\* are capable of constraining the last two higher-order expansion parameters of the black hole described by PRZ spacetime. We must ensure, however, that the constraints we obtained are the best-fit constraints on the expansion parameters (i.e.,  $\alpha$  and  $\lambda$ ). To do this, one has to consider observational data from the immediate vicinity of the black hole, where  $M/r_+$  should be smaller. Recently, some S-stars (S4711, S62, S4714) orbiting the supermassive black hole in Sgr A\* on short orbital periods ( $7.6 \text{ yr} \leq P_b \leq 12 \text{ yr}$ ) were discovered (Peißker et al. 2020). These stars have the potential to be used for measuring the general relativistic Lense-Thirring (LT) precessions (Iorio 2020; Iorio 2023). The forthcoming direct measurement of the periastron shift of these stars could lead to tighter constraints on our model parameters, even for nonspherically symmetric spacetime. In addition to S-stars, we will also consider the observational data of the selected microquasars, which are well-known as astrophysical quasiperiodic oscillations in the close vicinity of the black holes, where the condition  $M/r_+ \sim 10^{-1}$  is met. We intend to investigate this next in this paper.

### 5. Limits on the Parameters of PRZ Spacetime via Quasiperiodic Oscillations

In this section, we are concerned with motion perturbations around stable circular orbits. These perturbations are quasiperiodic oscillations (QPOs), the frequencies of which have direct observational effects (Strohmayer 2001; Barret et al. 2005; Török et al. 2005; Shafee et al. 2006; Kotrlóva et al. 2008; McClintock et al. 2011; Belloni et al. 2012; Azreg-Aïnou et al. 2020). We focus on the case of perturbed circular motion because it faithfully represents the trajectories of infalling matter in accretion processes.

From now on, we consider stable paths in the  $\theta = \pi/2$  plane. Epicyclic motion on a stable circular path has two components: one is a radial component in the equatorial plane, and the other one is a vertical component perpendicular to that plane. Instead of restricting ourselves to a special spherically symmetric metric, we consider for simplicity its most general form for the further analysis,

$$ds^2 = -g_{tt}(r)dt^2 + g_{rr}(r)dr^2 + g_{\theta\theta}(r)d\Omega^2. \quad (68)$$

The details of the derivations are given in Aliev & Galtsov (1981) and Azreg-Aïnou et al. (2020) for special static metrics and in Azreg-Aïnou (2019) for rotating metrics. Upon

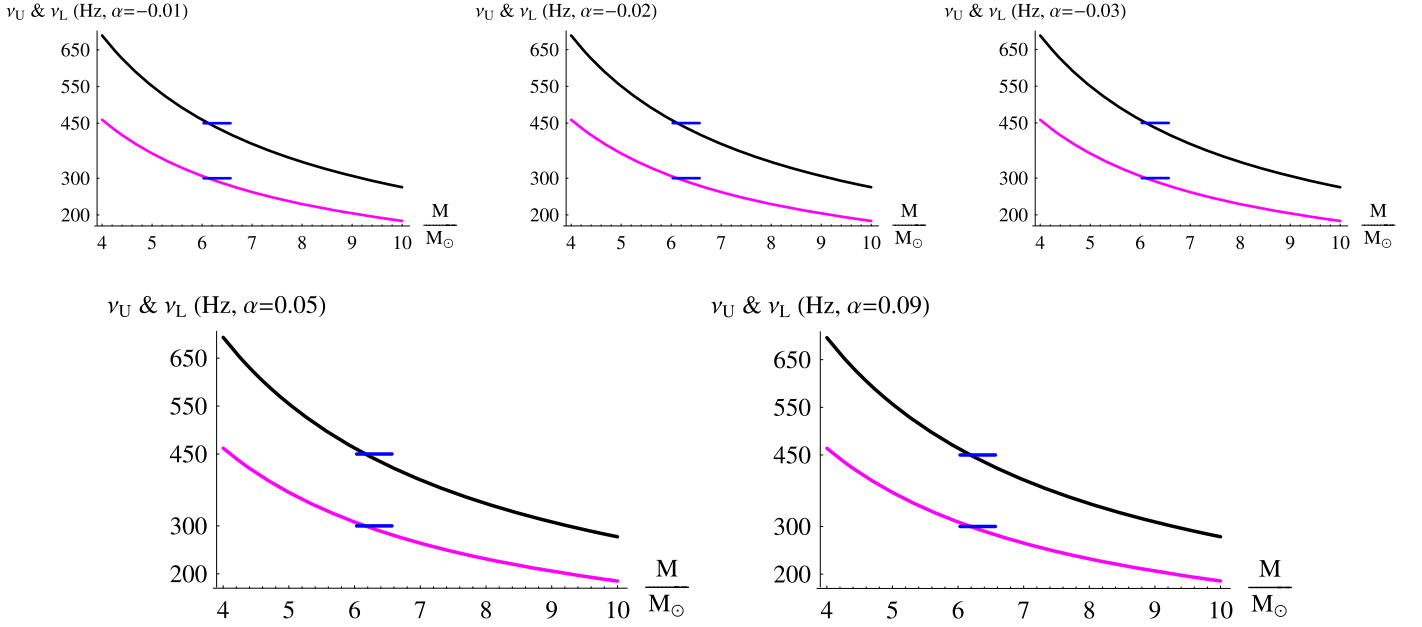


**Figure 4.** Curve fit to the data of the GRO J1655-40 Galactic microquasar (see Equation (76)). The black curves represent  $\nu_U = \nu_\theta + \nu_r$ , the magenta curves represent  $\nu_L = \nu_\theta$ , and the blue lines represent the uncertainty on the mass of the GRO J1655-40 microquasar. For these plots, we took  $\gamma = 1 + 2.3 \times 10^{-5}$ ,  $\beta = 1 + 2.3 \times 10^{-4}$ ,  $\lambda = 0.06$ , and the values of  $\alpha$  are shown in the plots.

following the same steps of the derivation, we arrive at

$$\nu_r = \frac{1}{2\pi} \sqrt{\frac{2g_{\theta\theta}(g'_{tt})^2 - 2g_{tt}g'_{tt}g'_{\theta\theta} - g_{tt}g_{\theta\theta}g''_{tt}}{2g_{tt}g_{rr}g_{\theta\theta}}} + \frac{g'_{tt}g''_{\theta\theta}}{2g_{rr}g'_{\theta\theta}}, \quad (69)$$

$$\nu_\theta = \frac{1}{2\pi} \sqrt{\frac{-g'_{tt}}{g'_{\theta\theta}}}, \quad (70)$$

where the prime notation denotes the derivative with respect to  $r$ . Here,  $\nu_r$  and  $\nu_\theta$  are the frequencies of the perturbed circular motion as detected by an observer at spatial infinity, which are related to the local frequencies,  $\Omega_r$  and  $\Omega_\theta$ , by  $\nu_r = \Omega_r/(2\pi u^t)$  and  $\nu_\theta = \Omega_\theta/(2\pi u^t)$ , where  $u^t$  and  $u^\varphi$  are the only nonvanishing components of the four-velocity vector of the infalling particle. Expressions similar to Equations (69) and (70) in the presence of a magnetic source were derived in Shaymatov et al. (2022).

For the case of the spherically symmetric metric we are considering in this work, Equations (1), (11), and (12), we have

$$g_{tt}(r) = -c^2 \left( 1 - \frac{2r_g}{r} + (\beta - \gamma) \frac{2r_g^2}{r^2} + \alpha \frac{2r_g^3}{r^3} \right), \quad (71)$$

$$g_{rr}(r) = 1 + \gamma \frac{2r_g}{r} + \lambda \frac{2r_g^2}{r^2}, \quad (72)$$

$$g_{\theta\theta}(r) = r^2, \quad (73)$$

where  $r_g = GM/c^2$ , and  $c$  and  $G$  are known physical constants taking the values in the SI system of  $299792458$  and  $6.673 \times 10^{-11}$ , respectively. To be consistent with the expansions in Equations (11) and (12), we only keep the following terms in the expansions of  $\nu_r$  and  $\nu_\theta$  in terms of the

dimensionless variable  $y = r/r_g$ :

$$\nu_r = \frac{c^3}{2\pi GM y^{3/2}} \times \left( 1 - \frac{2 + \gamma}{y} + \frac{3\gamma(\gamma - 4) + 3(\alpha - 4) + 2(8\beta - \lambda)}{2y^2} \right), \quad (74)$$

$$\nu_\theta = \frac{c^3}{2\pi GM y^{3/2}} \left( 1 - \frac{\beta - \gamma}{y} - \frac{3\alpha + (\beta - \gamma)^2}{2y^2} \right). \quad (75)$$

The two peaks in the power spectra from the GRO J1655-40 Galactic microquasar,

$$\begin{aligned} \text{GRO J1655 - 40: } \frac{M}{M_\odot} &= 6.30 \pm 0.27, \\ \nu_U &= 450 \pm 3 \text{ Hz}, \quad \nu_L = 300 \pm 5 \text{ Hz}, \end{aligned} \quad (76)$$

are at 300 Hz and 450 Hz (Strohmayer 2001). These two twin values of the QPOs are most certainly due to the phenomenon of resonance, which is due to the coupling of nonlinear vertical and radial oscillatory motions (Abramowicz et al. 2003; Horák & Karas 2006). The main three models for resonances (Abramowicz et al. 2003; Rebusco 2004; Deligianni et al. 2021; Banerjee 2022) are parametric resonance, forced resonance, and Keplerian resonance. There are other models as well (Banerjee 2022). In all three main models,  $\nu_U$  and  $\nu_L$  are linear combinations of the frequencies  $\nu_r$  and  $\nu_\theta$  detected by an observer at spatial infinity. The observed ratio  $\nu_U/\nu_L = 3/2$  can be compared with theory by making different assumptions within a resonance model.

The parameters  $\gamma$ ,  $\beta$ ,  $\alpha$ , and  $\lambda$ , as determined in the previous sections, have almost identical values to those of the Schwarzschild solution. We know from previous studies (Kološ et al. 2015) that parametric resonance is not able to justify the two twin peaks at 300 Hz and 450 Hz if the GRO J1655-40 microquasar is modeled by a Schwarzschild black

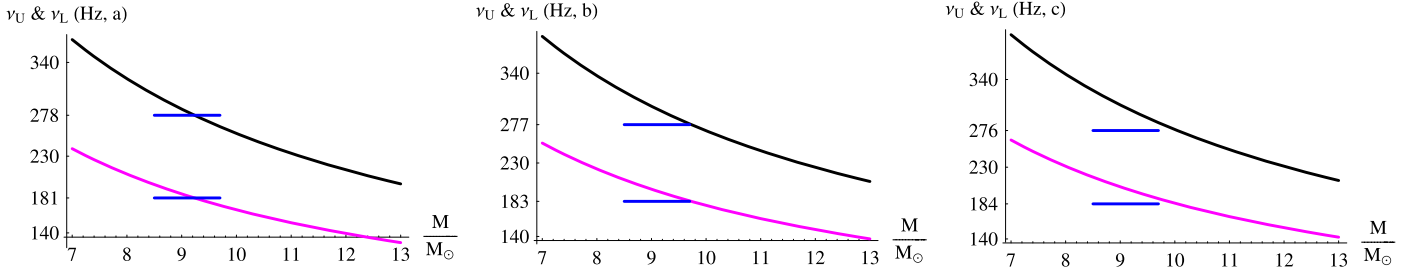


**Figure 5.** Curve fit to the data of the XTE J1550-564 Galactic microquasar (see Equation (79)). The black curves represent  $\nu_U = \nu_\theta + \nu_r$ , the magenta curves represent  $\nu_L = \nu_\theta$ , and the blue lines represent the uncertainty on the mass of the XTE J1550-564 microquasar. For these plots, we took  $\gamma = 1 + 2.3 \times 10^{-5}$ ,  $\beta = 1 + 2.3 \times 10^{-4}$ ,  $\lambda = 0.06$ , and  $\alpha = 0.05$ . Observing the new constraint, panels (a), (b), and (c) correspond to  $(\nu_U = 278 \text{ Hz and } \nu_L = 181 \text{ Hz})$ ,  $(\nu_U = 277 \text{ Hz, } \nu_L = 183 \text{ Hz})$ , and  $(\nu_U = 276 \text{ Hz, } \nu_L = 184 \text{ Hz})$ , respectively.

hole unless the effects of a magnetic field surrounding the black hole are taken into consideration. Thus, we opt for forced resonance (Deligianni et al. 2021; Banerjee 2022) with the model

$$\nu_U = \nu_\theta + \nu_r, \quad \nu_L = \nu_\theta, \quad (77)$$

which provides better results than the other models, i.e.,  $\nu_U = \nu_\theta$  and  $\nu_L = \nu_\theta - \nu_r$ . We use a graphical presentation, i.e., we plot  $\nu_U$  and  $\nu_L$  in terms of the mass ratio  $M/M_\odot$  for the value of the radial coordinate satisfying  $\nu_U/\nu_L = 450/300 = 3/2$  and fixed  $(\gamma, \beta, \alpha)$ , and we observe that the curves representing  $\nu_U$  and  $\nu_L$  cross the mass error band of the GRO J1655-40 microquasar (see, e.g., Kološ et al. 2015). For better results, we have selected this microquasar, which has the narrowest mass band error  $\Delta M = 0.54M_\odot$  (see Equation (76)). All panels of Figure 4 clearly depict the results. The black curves represent  $\nu_U = \nu_\theta + \nu_r$ , and the magenta curves represent  $\nu_L = \nu_\theta$  given in Equation (77), and the blue lines represent the uncertainty on the mass of the GRO J1655-40 microquasar. For these plots, we have taken  $\gamma = 1 + 2.3 \times 10^{-5}$ ,  $\beta = 1 + 2.3 \times 10^{-4}$ ,  $\lambda = 0.06$ , and the values of  $\alpha$  are shown in the plots. From Figure 4, one can observe that the values of  $\alpha$ ,

$$-0.03 \leq \alpha \leq 0.09, \quad (78)$$

offer a better curve fitting.

When the constraint in Equation (78) is admitted, one can move one step further in constraining the parameters of some other microquasars, e.g., the frequencies of the two peaks in the power spectra. The next microquasar with a well-constrained mass is XTE J1550-564 with  $\Delta M = 1.2M_\odot$ , which is given as

$$\begin{aligned} \text{XTE J1550 - 564: } \frac{M}{M_\odot} &= 9.1 \pm 0.6, \\ \nu_U &= 276 \pm 3 \text{ Hz, } \nu_L = 184 \pm 5 \text{ Hz.} \end{aligned} \quad (79)$$

Let the mass of the microquasar be in the middle of the mass band,  $M = 9.1M_\odot$ . We assume that the constraints given in Equation (78) hold well. In doing so, we further show in panel a of Figure 5 that the values

$$\nu_U = 278 \text{ Hz and } \nu_L = 181 \text{ Hz} \quad (80)$$

offer a better curve fitting for the XTE J1550-564 microquasar than the values  $\nu_U = 276 \text{ Hz}$  and  $\nu_L = 184 \text{ Hz}$ , which are in the middle of the frequency bands, as panel c of Figure 5 depicts. In panel b, we show that the curve fitting improves progressively upon departing from the middle values in the

frequency band, and when the values  $\nu_U = 278 \text{ Hz}$  and  $\nu_L = 181 \text{ Hz}$  are adopted.

From the analysis, we can infer that the obtained constraint values through the observations of QPOs in the black hole vicinity also satisfy the best-fit constraint values obtained by applying the observations of star S2 phenomena around Sgr A\*.

## 6. Conclusion

To test the extended theories of gravity, parameterization plays an important role in mimicking various gravity theories by using an expansion of the metric functions in terms of small dimensionless parameters. Therefore, in order to have constraints on the expansion parameters of spacetime from observation data, it becomes increasingly important to exploit the information obtained from classical solar system tests, the observations of phenomena of star S2, which is located in the star cluster close to Sgr A\*, and microquasars. With this in view, one may be able to obtain information about spacetime geometry near the horizon.

In this paper, we expanded the functions of the radial coordinate of spherically symmetric PRZ spacetime and found the higher-order expansion parameters  $\alpha$  and  $\lambda$ , which extend beyond the first-order PPN parameters. We then studied the constraints on the parameters of spherically symmetric PRZ spacetime through classical tests of SS effects, the data of star S2, which orbits Sgr A\*, and the data from the GRO J1655-40 and XTE J1550-564 microquasars. We determined the analytical expressions for SS effects, e.g., the perihelion shift, the light deflection, the gravitational time delay, and the QPO frequencies, to determine constraints on the higher-order expansion parameters of spherically symmetric PRZ spacetime (Rezzolla & Zhidenko 2014). We found the constraints on the two expansion parameters  $\alpha$  and  $\lambda$ , which survive only in the vicinity of the horizon by using the abovementioned three different observational data and approaches.

We further considered the impact of the expansion parameters of PRZ spacetime on the orbit of star S2, which orbits Sgr A\* at the center of the Milky Way galaxy, which can provide excellent tests in probing black hole properties. We also considered the effects of PRZ spacetime to compare them with the astrometric and spectroscopic data that are publicly available and involve the astrometric positions, the radial velocities, and the orbital precession for star S2 considered in this paper. Taking all together, we applied the MCMC simulations to probe the possible effects of these expansion parameters on the orbit of star S2 and the constraints on the parameters of spherically symmetric PRZ spacetime. We found the best-fit constraint values through the corresponding

posterior distribution of the expansion parameters, which can be observationally constrained to be  $\beta = 1.03^{+0.32}_{-0.35}$ ,  $\gamma = 0.93^{+0.28}_{-0.25}$  and  $\alpha, \lambda = (-0.09, 0.09)$  at the 90% confidence level. However, we found that the observational constraints on  $\alpha$  and  $\lambda$  are more accurate than that of SS tests and that have significant impact on the orbit of star S2. Therefore, it was shown that the observational data for star S2, which orbits Sgr A\*, can constrain the expansion parameters of PRZ spacetime, thus allowing one to obtain the best-fit constraint region on the expansion parameters  $\alpha$  and  $\lambda$ .






To confirm what we obtained through observational data for star S2, we also considered observational data in the close vicinity of the black hole, i.e.,  $M/r_+ \sim 10^{-1}$  was always satisfied, which is comparable with the orbit of star S2 around Sgr A\*. Therefore, we studied the epicyclic motions and derived the analytic form of the epicyclic frequencies used to constrain these expansion parameters of PRZ spacetime by applying data of the selected microquasars that are well-known as astrophysical QPOs, which are interesting tools for testing and constraining the geometry of metric fields because, as noted in Banerjee (2022), their frequencies solely depend on the spacetime metric and not on the details of the accretion process. Even the radius of the ISCO where accretion occurs only depends on the background metric, provided the energy-momentum tensor of the fluid is seen as a test matter. From this point of view, QPOs provide deeper insights into the background metric. Thus, observations of QPOs have been used as very potent tests in probing the unknown aspects associated with precise measurements and constraints of the parameters of black holes. Further, we obtained constraints on the higher-order expansion parameters of PRZ spacetime and constraints on the frequencies of the two peaks in the power spectra of the GRO J1655-40 and XTE J1550-564 microquasars. We showed that the obtained best-fit constraint values through observations of phenomena of star S2 are well satisfied by the observations of QPOs in the vicinity of the black hole.

Finally, taking into consideration all results, we can state that these two higher-order expansion parameters would be in the range  $\alpha, \lambda = (-0.09, 0.09)$  and  $\sim 10^{-2}$  as inferred from the observations of SS tests, star S2, which orbits Sgr A\*, and QPOs around a black hole. As a consequence, our results suggest that the higher-order expansion parameters  $\alpha$  and  $\lambda$  would survive only in the vicinity of a black hole horizon in the strong-field regime.

### Acknowledgments

This work is supported by the National Natural Science Foundation of China under grants No. 11675143 and No. 11975203, the National Key Research and Development Program of China under grant No. 2020YFC2201503. B.A. wishes to acknowledge the support from Research F-FA-2021-432 of the Uzbekistan Ministry for Innovative Development.

### ORCID iDs

Bobomurat Ahmedov  <https://orcid.org/0000-0002-1232-610X>  
 Mariafelicia De Laurentis  <https://orcid.org/0000-0002-9945-682X>  
 Mubasher Jamil  <https://orcid.org/0000-0001-9662-1546>  
 Qiang Wu  <https://orcid.org/0000-0002-3345-9905>  
 Anzhong Wang  <https://orcid.org/0000-0002-8852-9966>

### References

- Abbott, B. P., LIGO Scientific Collaborations, Virgo Scientific Collaborations, et al. 2016, *PhRvL*, **116**, 061102
- Abramowicz, M. A., Karas, V., Kluzniak, W., Lee, W. H., & Rebusco, P. 2003, *PASJ*, **55**, 467
- Akiyama, K., Alberdi, A., Event Horizon Telescope Collaboration, et al. 2019a, *ApJL*, **875**, L1
- Akiyama, K., Alberdi, A., Event Horizon Telescope Collaboration, et al. 2019b, *ApJL*, **875**, L6
- Akiyama, K., Alberdi, A., Event Horizon Telescope Collaboration, et al. 2022, *ApJL*, **930**, L12
- Aliev, A. N., Esmer, G. D., & Talazan, P. 2013, *CQGra*, **30**, 045010
- Aliev, A. N., & Galtsov, D. V. 1981, *GRGr*, **13**, 899
- Azreg-Ainou, M. 2019, *IJMPD*, **28**, 1950013
- Azreg-Ainou, M., Chen, Z., Deng, B., et al. 2020, *PhRvD*, **102**, 044028
- Bambi, C. 2012, *PhRvD*, **85**, 043002
- Bambi, C., Jiang, J., & Steiner, J. F. 2016, *CQGra*, **33**, 064001
- Banerjee, I. 2022, *JCAP*, **2022**, 034
- Barret, D., Olive, J.-F., & Miller, M. C. 2005, *MNRAS*, **361**, 855
- Becerra-Vergara, E. A., Argüelles, C. R., Krut, A., Rueda, J. A., & Ruffini, R. 2020, *A&A*, **641**, A34
- Belloni, T. M., Sanna, A., & Méndez, M. 2012, *MNRAS*, **426**, 1701
- Bertotti, B., Iess, L., & Tortora, P. 2003, *Nature (London)*, **425**, 374
- Caldwell, R., & Kamionkowski, M. 2009, *Natur*, **458**, 587
- Carloni, S., Grumiller, D., & Preis, F. 2011, *PhRvD*, **83**, 124024
- De Laurentis, M., Younsi, Z., Porth, O., Mizuno, Y., & Rezzolla, L. 2018, *PhRvD*, **97**, 104024
- Deligianni, E., Kleihaus, B., Kunz, J., Nedkova, P., & Yazadjiev, S. 2021, *PhRvD*, **104**, 064043
- Di Valentino, E., Mena, O., Pan, S., et al. 2021, *CQGra*, **38**, 153001
- Do, T., Hees, A., Ghez, A., et al. 2019, *Sci*, **365**, 664
- Dokuchaev, V. I., & Eroshenko, Y. N. 2015, *PhyU*, **58**, 772
- Einstein, A. 1916, *AnP*, **354**, 769
- Foreman-Mackey, D., Hogg, D. W., Lang, D., & Goodman, J. 2013, *PASP*, **125**, 306
- Germanà, C. 2018, *PhRvD*, **98**, 083025
- Ghasemi-Nodehi, M., Azreg-Ainou, M., Jusufi, K., & Jamil, M. 2020, *PhRvD*, **102**, 104032
- Ghez, A. M., Klein, B. L., Morris, M., & Becklin, E. E. 1998, *ApJ*, **509**, 678
- Ghez, A. M., Morris, M., Becklin, E. E., Tanner, A., & Kremenek, T. 2000, *Natur*, **407**, 349
- Ghez, A. M., Salim, S., Hornstein, S. D., et al. 2005, *ApJ*, **620**, 744
- Gillessen, S., Plewa, P. M., Eisenhauer, F., et al. 2017, *ApJ*, **837**, 30
- Glampedakis, K., Pappas, G., Silva, H. O., & Berti, E. 2017, *PhRvD*, **96**, 064054
- GRAVITY Collaboration 2018, *A&A*, **615**, L15
- GRAVITY Collaboration 2020, *A&A*, **636**, L5
- Grumiller, D. 2010, *PhRvL*, **105**, 211303
- Hellerman, S., Kaloper, N., & Susskind, L. 2001, *JHEP*, **2001**, 003
- Horák, J., & Karas, V. 2006, *A&A*, **451**, 377
- Hulse, R. A., & Taylor, J. H. 1974, *ApJL*, **191**, L59
- Hulse, R. A., & Taylor, J. H. 1975, *ApJL*, **195**, L51
- Iorio, L. 2015, *IJMPD*, **24**, 1530015
- Iorio, L. 2019, *AJ*, **157**, 220
- Iorio, L. 2020, *ApJ*, **904**, 186
- Iorio, L. 2023, *ApJ*, **954**, 219
- Johannsen, T., & Psaltis, D. 2011, *PhRvD*, **83**, 124015
- Jusufi, K., Azreg-Ainou, M., Jamil, M., et al. 2021, *PhRvD*, **103**, 024013
- Jusufi, K., Azreg-Ainou, M., Jamil, M., & Saridakis, E. N. 2022a, *Univ. J*, **8**, 102
- Jusufi, K., Kumar, S., Azreg-Ainou, M., et al. 2022b, *EPJC*, **82**, 633
- Kagramanova, V., Kunz, J., & Lämmerzahl, C. 2006, *PhLB*, **634**, 465
- Kiselev, V. V. 2003, *CQGra*, **20**, 1187
- Kluzniak, W., & Abramowicz, M. A. 2001, *AcPPB*, **32**, 3605
- Kološ, M., Stuchlík, Z., & Tursunov, A. 2015, *CQGra*, **32**, 165009
- Konoplya, R., Rezzolla, L., & Zhidenko, A. 2016, *PhRvD*, **93**, 064015
- Kotrlová, A., Stuchlík, Z., & Török, G. 2008, *CQGra*, **25**, 225016
- Lacroix, T. 2018, *A&A*, **619**, A46
- McClintock, J. E., Narayan, R., Davis, S. W., et al. 2011, *CQGra*, **28**, 114009
- Nampalliwar, S., Kumar, S., Jusufi, K., et al. 2021, *ApJ*, **916**, 116
- Nucita, A. A., De Paolis, F., Inghrosso, G., Qadir, A., & Zakharov, A. F. 2007, *PASP*, **119**, 349
- Pánis, R., Kološ, M., & Stuchlík, Z. 2019, *EPJC*, **79**, 479
- Peebles, P. J., & Ratra, B. 2003, *RvMP*, **75**, 559
- Peißker, F., Eckart, A., Zajaček, M., Ali, B., & Parsa, M. 2020, *ApJ*, **899**, 50
- Perlick, V., & Tsupko, O. Y. 2022, *PhR*, **947**, 1

- Persic, M., Salucci, P., & Stel, F. 1996, *MNRAS*, **281**, 27
- Rayimbaev, J., Majeed, B., Jamil, M., Jusufi, K., & Wang, A. 2022, *PDU*, **35**, 100930
- Rayimbaev, J., Shaymatov, S., & Jamil, M. 2021, *EPJC*, **81**, 699
- Rebusco, P. 2004, *PASJ*, **56**, 553
- Reid, M. J., Menten, K. M., Trippe, S., Ott, T., & Genzel, R. 2007, *ApJ*, **659**, 378
- Rezzolla, L., Yoshida, S., Maccarone, T. J., & Zanotti, O. 2003, *MNRAS*, **344**, L37
- Rezzolla, L., & Zhidenko, A. 2014, *PhRvD*, **90**, 084009
- Rubin, V. C., Ford, W. K. J., & Thonnard, N. N. 1980, *ApJ*, **238**, 471
- Shafee, R., McClintock, J. E., Narayan, R., et al. 2006, *ApJL*, **636**, L113
- Shapiro, S. S., Davis, J. L., Lebach, D. E., & Gregory, J. S. 2004, *PhRvL*, **92**, 121101
- Shaymatov, S., Jamil, M., Jusufi, K., & Bamba, K. 2022, *EPJC*, **82**, 636
- Shaymatov, S., Vrba, J., Malafarina, D., Ahmedov, B., & Stuchlík, Z. 2020, *PDU*, **30**, 100648
- Spergel, D. N., Bean, R., Doré, O., et al. 2007, *ApJS*, **170**, 377
- Stella, L., Vietri, M., & Morsink, S. M. 1999, *ApJL*, **524**, L63
- Strohmayer, T. E. 2001, *ApJL*, **552**, L49
- Stuchlík, Z., Slany, P., & Torok, G. 2007, *A&A*, **470**, 401
- Tarnopolski, M., & Marchenko, V. 2021, *ApJ*, **911**, 20
- Tasheva, R. P., & Stefanov, I. Z. 2019, in AIP Conf. Proc. 2075, 10th Jubilee Int. Conf. of the Balkan Physical Union (Melville, NY: AIP), 090007
- Titarchuk, L., & Shaposhnikov, N. 2005, *ApJ*, **626**, 298
- Török, G., Abramowicz, M. A., Kluźniak, W., & Stuchlík, Z. 2005, *A&A*, **436**, 1
- Tripathi, A., Yan, J., Yang, Y., et al. 2019, *ApJ*, **874**, 135
- Tursunov, A., Stuchlík, Z., Kološ, M., Dadhich, N., & Ahmedov, B. 2020, *ApJ*, **895**, 14
- Wald, R. M. 1984, *General Relativity* (Chicago, IL: Univ. Chicago Press)
- Weinberg, S. 1972, *Gravitation and Cosmology: Principles and Applications of the General Theory of Relativity* (New York: Wiley)
- Wetterich, C. 1988, *NuPhB*, **302**, 668
- Will, C. M. 1993, *Theory and Experiment in Gravitational Physics*, Vol. 396 (Cambridge: Cambridge Univ. Press)
- Will, C. M. 2001, *LRR*, **4**, 4
- Will, C. M. 2006, *LRR*, **9**, 3
- Yan, J.-M., Wu, Q., Liu, C., Zhu, T., & Wang, A. 2022, *JCAP*, **2022**, 008
- Yang, S., Liu, C., Zhu, T., et al. 2021, *ChPhC*, **45**, 015102